Investigation of the influence of engine settings on the heat flux in a hydrogen- and methane-fueled spark ignition engine

Demuynck, Joachim, De Paepe Michel, Huisseune, Henk, Sierens, Roger, Vancoillie, Jeroen, Verhelst, Sebastian

In: APPLIED THERMAL ENGINEERING, 31 (6-7), pp 1220-1228, 2011

http://dx.doi.org/10.1016/j.applthermaleng.2010.12.023

Investigation of the influence of engine settings on the heat flux in a hydrogen- and methane-fuelled spark ignition engine

Joachim Demuynck, Michel De Paepe, Henk Huisseune, Roger Sierens, Jeroen Vancoillie, Sebastian Verhelst

Ghent University, Department of Flow, Heat and Combustion Mechanics, Sint-Pietersnieuwstraat 41 B-9000 Gent, Belgium

Abstract

Hydrogen-fuelled internal combustion engines are a possible solution to make transportation more ecological. Only emissions of oxides of nitrogen (NO_x) occur at high loads, being a constraint for power and efficiency optimization. A thermodynamic model of the engine cycle enables a cheap and fast optimization of engine settings. It needs to accurately predict the heat transfer in the engine because the NO_x emissions are influenced by the maximum gas temperature. However, The existing engine heat transfer models in the literature are developed for fossil fuels and they have been cited to be inaccurate for hydrogen. We have measured the heat transfer inside a spark ignited engine with a thermopile to investigate the heat transfer process of hydrogen and to find the differences with a fossil fuel. This paper describes the effects of the compression ratio, ignition timing and mixture richness on the heat transfer process, comparing hydrogen with methane. A convection coefficient is used to separate the effect of the temperature difference between the gas and the wall from the influence of the gas movement and combustion. The paper shows that the convection coefficient gives more insight in the heat transfer process in a combustion engine despite the assumptions involved in its definition. The comparison between hydrogen and methane demonstrates, in contrast to what is believed, that the heat loss of hydrogen can be lower.

Keywords: hydrogen, methane, internal combustion engine, experimental, heat transfer, thermopile

Nomenclature

Abbreviations

°CA degree crank angle

*Corresponding author. Tel.: +32(0)92643302; Fax: +32(0)92643590
Email address: joachim.demuynck@ugent.be (Joachim Demuynck)

NO_x	oxides of nitrogen
ABDC	after bottom dead centre
ATDC	after top dead centre
BBDC	before bottom dead centre
BTDC	before top dead centre
CFD	Computational Fluid Dynamics
CFR	Cooperative Fuel Research
EGR	exhaust gas recirculation
EVC	exhaust valve closure
EVO	exhaust valve opening
FS	full scale
GUEST	Ghent University engine simulation tool
HCCI	homogeneous charge compression ignition
HFM	heat flux microsensor
HFS	heat flux sensor
ICE	internal combustion engine
IGN	ignition timing
IMEP	indicated mean effective pressure
IVC	intake valve closure
IVO	intake valve opening
MBT	minimum spark advance for maximum brake torque
PFI	port fuel injection
RTD	resistance temperature detector
RTS	resistance temperature sensing
SA	sample signal
TRIG	trigger signal
WOT	wide open throttle

Greek symbols

ϵ compression ratio

η_i indicated thermal efficiency

λ air-to-fuel equivalence ratio

ϕ_h cooling loss ratio

θ crank angle

Roman Symbols

Q_a apparent heat release, $[J/°CA]$

Q_h total cycle heat loss, $[J]$

Q_f total heat released during combustion, $[J]$

W_i indicated work, $[J]$

1. Introduction

Climate change and energy supply both are issues high on the political agenda these days. A solution has to be found to move away from the fossil fuel based energy supply of today. The transportation sector in particular is very dependent on fossil fuels. Therefore, researchers have tried to find alternative fuels for several years.

The hydrogen-fuelled combustion engine is one of the possible alternatives which is investigated at the Transportation Technology group at Ghent University. These engines are an attractive alternative for the current drive trains because the combustion properties of hydrogen enable a high efficiency for all engine loads by using several operational strategies [1]. Moreover, hydrogen engines have near-zero noxious and zero greenhouse gas emissions at the tailpipe. The initial research at Ghent University was focused on the experimental optimization of engine operational strategies for maximum power and efficiency, with ultra low emissions of oxides of nitrogen (NO_x) [2–4]. The focus shifted to numerical research with the development of a thermodynamic model of the engine cycle, called the GUEST-code (Ghent University Engine Simulation Tool) [5, 6].

Such a thermodynamic model of the engine cycle enables a cheap and fast optimization of engine settings for operation on hydrogen. Several submodels are necessary to solve the conservation equations of energy and mass: a combustion, a turbulence and a heat transfer model among other things. The last one is important to accurately simulate the NO_x emissions which are influenced by the maximum gas temperature. These emissions can occur in hydrogen internal combustion engines at high loads, being an important constraint for power and efficiency optimization.

A lot of research has been performed on the heat transfer in engines, but clear results remain scarce. Consequently, several research groups are still looking into it, e.g. [7–11]. Experimental investigations were mainly done between 1970 and 1990 and the

focus has shifted towards numerical work. The results of CFD (Computational Fluid Dynamics) codes are validated with the available measurements in the literature [12] or compared with simulation results of semi-empirical models [13]. The agreement with the measurements is poor, therefore, efforts focus on the development of new wall functions [12, 14, 15]. Quasi-dimensional models for the engine cycle are still the standard, using semi-empirical submodels for the heat transfer. The latter were mainly developed before 1990 and are reported to be inaccurate for new combustion types like HCCI (Homogeneous Charge Compression Ignition) [16–18] and alternative fuels like hydrogen [19–21]. Consequently, experimental research is still needed to understand the heat transfer process inside modern combustion engines.

We are investigating experimentally the differences in the heat transfer of hydrogen and fossil fuels (in this case methane) in order to improve the existing heat transfer models. Several methods to measure the heat flux in an internal combustion engine exist, but new types are still being developed as well [22]. Therefore, one of the purposes of our research is to compare several sensors based on the measurement accuracy and construction feasibility as described in [23]. One of the selected sensors has been used to measure heat transfer rates and wall temperatures in a spark ignition engine [24]. A convection coefficient is now used to gain more insight into those measurements. This paper first describes an investigation of motored measurements. Then, it presents the effects of the compression ratio, ignition timing and mixture richness on fired measurements. The paper ultimately compares measurements of hydrogen and methane with the same indicated power output.

2. Experimental method

2.1. Equipment

An overview of the test setup is shown in Figs. 1 and 2. The engine used in this research is a four-stroke single-cylinder spark ignited gas engine based on a CFR (Co-operative Fuel Research) engine operated at a constant speed of 600 rpm. It is equipped with PFI (port fuel injection) and has a variable compression ratio. The details of the engine are given in Table 1. Fuel injection and ignition timing are controlled by a *MoTeC M4Pro* electronic control unit.

The heat flux measurements were carried out with a *Vatell HFM-7* sensor which consists of a thermopile (heat flux signal, HFS) and an RTD (substrate temperature signal, RTS). The sensor has a response time of 17 µs. The *Vatell AMP-6* amplifier was used as a current source for the RTD and as an amplifier for both output signals. The sensor is calibrated by Vatell (see below) and it has been used before to measure the heat flux in the intake manifold [25–27] and the cylinder [27] of an internal combustion engine.

As the test engine is easily accessible, the heat flux sensor was successively installed in three different positions under fired operation (P2, P3, P4 as shown in Fig. 1). These openings are at the same height in the cylinder wall and are equally distributed around the circumference of the cylinder. The spark plug was placed in position P1. The heat flux sensor could be mounted in P1 as well in the case of motored operation, because of the absence of the spark plug. The measurement position is mentioned in the caption of all the figures in the following sections.

In-cylinder pressures were measured with a water-cooled *Kistler 701A* piezoelectric pressure sensor (in P2 or P4) and inlet pressure with a *Kistler 4075A20* piezoresistive pressure sensor. This inlet pressure was used to reference in-cylinder pressure. A 12 bit data acquisition card was used to sample both the heat flux and pressure signals. It is triggered by a crank angle encoder every 0.5 °CA, resulting in a sampling rate of 7.2 kHz. Next, Gas flows were measured with *Bronkhorst Hi-Tec F-201AC* (fuel) and *F-106BZ* (air) flow sensors. Finally, type K thermocouples were used to measure inlet and exhaust gas temperatures.

2.2. Data reduction

Most of the literature concerning engine heat transfer calculates a convection coefficient (h) out of the measured heat flux (q) and the difference between the gas temperature (T_g) and the wall temperature (T_w) with equation 1. This equation is actually only valid for steady convection, so the heat transfer process in the engine has to be assumed to be quasi-steady. This means that the instantaneous heat flux is proportional to the instantaneous temperature difference between the gas and the wall. This concept is not entirely justifiable because the heat transfer in an engine is transient and there is a time lag between the temperature difference and the heat flux due to the heat capacity of the gas [28]. However, an alternative approach has not been proposed so far, so we have calculated a time-resolved convection coefficient with equation 1, evaluating the insight it provides.

$$h = \frac{q}{(T_g - T_w)} \tag{1}$$

The idea is to separate the temperature difference between the gas and the wall from other influencing factors on the heat transfer process. The convection coefficient represents the influence of the gas velocity, the turbulence, the propagating flame front and the gas properties (Prandtl number, viscosity, conductivity and heat capacity). It will be shown further on that the convection coefficient gives more information than the heat flux trace alone.

The combustion gases are assumed to behave like ideal gases. Therefore, the bulk gas temperature is calculated with the following equation of state: $T_g = p \cdot V/m \cdot R$. The in-cylinder pressure (p) is measured and the volume (V) can be calculated out of the crank position. The mass (m) can only be determined during the closed part of the combustion cycle, being the sum of the measured incoming mass (air and fuel) and the residuals and neglecting blow-by effects because of the large number of piston rings (5). No incoming mass goes directly to the exhaust manifold because the test engine does not have a valve overlap. The residual mass is therefore determined with the equation of state at EVC (exhaust valve closure) using the measured cylinder pressure and assuming that the in-cylinder temperature is equal to the measured exhaust temperature. The specific gas constant (R) at IVC (intake valve closure) can be calculated out of the mass average of the specific gas constants of the air, the fuel and the residual gases. This value is used until the beginning of the combustion. At the end of the combustion R is equal to that of the combustion products. In between, the specific gas constant is calculated with a linear interpolation. The moment where the combustion begins and ends is determined with an apparent rate of heat release analysis.

An indication of total cycle heat losses (Q_h) is calculated, assuming that the measured heat flux trace at the measurement position occurs evenly over the entire cylinder wall. The measured heat flux is multiplied with the total available in-cylinder surface for each sampling point and all these values are summed up to get the total cycle heat loss.

2.3. Error analysis

To judge the quality of the measurement results, a thorough error analysis has been carried out following the methods described in Taylor [29]. The error analysis is based on the accuracy of the measurement equipment which is given in Table 2. The pressure measurement circuit is calibrated with a dead-weight tester in the laboratory. The given uncertainty of a pressure sensor is the standard deviation of the calibration which is repeated 50 times.

The HFM sensor is not included in Table 2 because its accuracy depends on several coefficients which are used to calculate the heat flux and wall temperature out of the measured HFS and RTS signal (see HFM manual [30]). These coefficients and their uncertainty are determined during the calibration of the sensor at the factory of Vatell. The resulting maximum relative error on the heat flux is 3 % during the compression and expansion stroke and 7 % during the intake and exhaust stroke. The maximum relative error on the wall temperature is 5 %.

The uncertainty on the compression ratio (ϵ) is negligible. The absolute error on the crank angle and ignition timing is 0.5 °CA. A change of 0.5 °CA causes a maximum change of 1 % in the calculated cylinder volume, so this is taken as the relative error on the cylinder volume. The maximum relative error on the gas flow rates is 4 % for air and hydrogen and 9 % for methane. The resulting error on the air-to-fuel equivalence ratio (λ) is 5 % for hydrogen and 10 % for methane.

The indicated work output (W_i) is calculated with an accuracy of 2.5 %. The uncertainty on the heat loss through the cylinder walls (Q_h) is estimated to be 7.6 %. The heat input of the fuel (Q_f) has a relative error of 9 % for methane and 4 % for hydrogen. The relative error on the indicated efficiency ($\eta_i = W_i/Q_f$) is 9.3 % for methane and 4.7 % for hydrogen. The maximum relative error on the heat loss ratio ($\phi_h = Q_h/Q_f$) is 11.8 % for methane and 8.6 % for hydrogen.

A change of 10 % in λ causes a change of 0.3 % in the calculated specific gas constant (R) of a methane-air mixture. Changing λ with 4 % changes the R of for a hydrogen-air mixture with 0.6 %. These errors on R are negligible. The maximum relative error on the calculated gas temperature is 6 %. The convection coefficient is calculated with an uncertainty of 11 %. These uncertainties are calculated assuming that the cylinder temperature at EVC is equal to the exhaust temperature as explained earlier. A sensitivity analysis has been performed to check the influence of the choice of this temperature. Varying the cylinder temperature at EVC with 20 % changes the residual gas fraction with 10 %, but the calculated bulk gas temperature and convection coefficient only change with 1 %. This influence is acceptable for the calculations in this paper.

3. Results and discussion

Measurements under motored conditions with a variation in the compression ratio and in-cylinder mass are discussed first. Then, fired measurements on hydrogen are presented. The compression ratio (ϵ), ignition timing (IGN) and air-to-fuel equivalence ratio (λ) were varied in that case. Ultimately, a comparison is made between hydrogen and methane measurements with the same indicated power output.

The measurements on hydrogen were performed with wide-open-throttle (WOT), varying the power by changing the air-to-fuel equivalence ratio. It is not possible to control the power output in a sufficient range by changing λ in the case of methane, so a throttle in the intake manifold was used. Ignition was at MBT-timing (minimum spark advance for Maximum Brake Torque), unless mentioned otherwise. The ignition timing is always indicated in the graphs.

This paper presents the heat flux traces of the ensemble cycle. The heat flux of the ensemble cycle at a certain crank angle is the average of all the heat fluxes of an entire measurement set at that crank angle. A measurement set always consisted of 35 cycles.

There are three elements in equation 1: the measured heat flux, the calculated convection coefficient and the temperature difference between the calculated gas and the measured wall temperature. These three elements will be plotted in the same graph throughout this paper. The heat flux will be plotted at the top, the temperature difference in the middle and the convection coefficient at the bottom.

3.1. Motored operation

The heat flux is first investigated in the engine under motored operation. In this case only air flows into the engine and there is no combustion. This allows to gain insight into the effect of the gas flow and turbulence on the heat transfer process, without the interference of the effect of a propagating flame front. Figure 3 shows that there are only small differences between the heat flux or convection coefficient at the different measurement positions, indicating that bulk processes mainly influence the heat flux under motored operation.

3.1.1. Variation of the compression ratio

The heat flux, the temperature difference and the convection coefficient for a variation in the compression ratio, with constant intake temperature and pressure, are plotted in Fig. 4. The heat flux and wall temperature are measured at P1. Overall, the traces peak just before TDC (top dead centre), shortly before the cylinder pressure peaks. The peak in the heat flux trace (at the top of the graph) rises if the compression ratio increases from 6 to 15, as expected. The maximum in the gas temperature increases from 375 °C to 475 °C, mainly because of the rise in the in-cylinder pressure. The wall temperature only increases by 12 °C. As a result, the peak temperature difference between the gas and the wall increases with the compression ratio. The increase in the heat flux cannot only be caused by the increasing ΔT, because the convection coefficient is significantly higher as well. Consequently, this confirms that gas motion and turbulence have an effect on the heat transfer.

Figure 4 shows that the trend is the other way around near the end of the expansion period, the heat flux decreases with an increasing compression ratio. This can partially

be explained by a decrease in ΔT which is caused by two effects. First, the gas temperature is lower (after 415 °CA) because the cylinder pressure is almost the same and the volume is smaller. Second, the wall temperature is almost constant during the cycle and thus still higher. Other effects must have an influence on the heat flux as well, because there is a larger difference in the traces of the convection coefficient.

The trace of h near the end of the expansion period demonstrates that the assumption of a quasi-steady heat transfer process is not justifiable, because the convection coefficients become negative.

3.1.2. Variation of the throttle position

A throttle is used in the intake manifold to investigate the effect of a reduced in-cylinder mass on the heat transfer. The throttle position can be varied between 0° and 90°. The effect of three throttle position on the cylinder pressure ($\epsilon = 10$) is plotted in Fig. 5. Varying its position until 65° does not have an influence, because the very low engine speed results in a small air flow rate. The corresponding q, ΔT and h at P1 are shown in Figure 6. The heat flux increases if the throttle opening is varied between 0° and 70°. This can partially be explained by an increase in the temperature difference between the gas and the wall. The turbulence caused by the throttle must have an influence as well and this effect is visible in the increased convection coefficient. The increase in the gas temperature for a decrease in the pressure is unexpected. However, the in-cylinder mass decreases as well and the ratio of p over m in the equation of state is higher as a consequence.

Further throttling reduces the trapped mass more which causes the cylinder pressure to drop significantly. Consequently, the gas temperature and the heat flux decrease. The convection coefficient decreases as well.

3.2. Fired operation

3.2.1. General observations

A typical trace of the wall temperature during an engine cycle under fired operation is plotted in Fig. 7 (at P2 with $\lambda = 1$ and $\epsilon = 8$). The wall temperature under motored operation is plotted as well to show the effect of combustion. Under fired operation, the wall temperature decreases somewhat during the intake stroke because of the incoming mixture of air and fuel which cools down the wall. The wall temperature then increases by 5 to 10 °C (depending on the engine operation point) during the combustion period and decreases again towards the end of the expansion stroke and during the exhaust stroke. In contrast, under motored condition the temperature almost remains constant over the entire engine cycle. The differences between the wall temperature with a change in the engine operation are the peak-to-peak value and the steady state level. The wall temperature will not be plotted any more in this paper. All the graphs will show the temperature difference (ΔT) between the gas and the wall ($T_g - T_w$, see equation 1) because this drives the heat transfer process.

The measured heat flux, the calculated convection coefficient and the temperature difference for a reference measurement are plotted in Fig. 8 to discuss the general observations. The measurement plotted is taken at P2, λ is equal to 1 and the compression ratio is 8.

Two vertical dotted lines are drawn on the graph. Line 1 corresponds with the maximum of the convection coefficient and line 2 coincides with the maximum of the temperature difference. The intersection of these two lines with the trace of the heat flux is of interest. Line 1 corresponds with the end of the initial steep rise in the heat flux trace. Line 2 coincides with the maximum in the heat flux trace. The maximum heat flux thus occurs at the moment that the temperature difference peaks. However, the initial increase in the heat transfer is mainly caused by the propagating flame front that passes over the measurement position. This effect is visible in the trace of the convection coefficient.

Although the definition of a convection coefficient is based on the assumption of a quasi-steady process, which is not the case as shown with the motored measurements, it gives more insight into the heat transfer process than the measured heat flux trace alone. The observations discussed in this section are valid for all the measurements plotted further on, where line 1 and 2 are inserted as well.

In contrast to the motored measurements, there are significant differences in the heat flux between the different measurement positions. Both the instant where the heat flux starts to increase and the peak value differ, caused by the difference in the arrival time of the propagating flame front, see [24]. For a variation in the measurement position, the trace of the convection coefficient does not provide extra insight, because the trace of the temperature difference is the same for all the positions.

3.2.2. Variation of the compression ratio

The compression ratio is varied from $\epsilon = 6$ to $\epsilon = 10$. The traces of q, ΔT and h are plotted in Fig. 9 (at P2 and $\lambda = 1.5$). The cylinder pressure of the three measurements is plotted in Fig. 10. The measurements have the same ignition timings (at TDC), so that only the compression ratio is varied.

There is an overall increase in the heat flux for a higher compression ratio, except near the end of the expansion stroke. According to Heywood [31] several operational properties change with an increasing ϵ: the gas pressure and peak burned gas temperature increase, gas motion increases, combustion is faster and the gas temperature late in the expansion stroke decreases. The first four properties increase the heat transfer, the last one decreases it. Fig. 9 shows that the peak in the difference between the gas temperature and the wall temperature does not increase with an increasing compression ratio for these measurements, which is also the case for the gas temperature itself. This is an unexpected result. The higher peak pressure for a higher compression ratio is in the calculation of T_g, with the equation of state, countered by the smaller in-cylinder volume, resulting in the same peak gas temperature. The cylinder volume is not only larger at the moment of maximum pressure because of the lower compression ratio, but also because of the fact that the pressure peaks later in the combustion cycle. However, the gas temperature is higher during the beginning of the combustion process, resulting in an increase in the heat flux after TDC. The temperature difference between the gas and the wall for a compression ratio of 6 eventually rises to the same maximum like for the higher compression ratios, boosting the heat flux around a crank angle of 380 °CA to a level which is higher than expected.

The difference in the maximum of the convection coefficient going from $\epsilon = 6$ to $\epsilon = 8$ is not significant. In contrast, there is a significant increase if ϵ is changed

between 8 and 10. Consequently, the increase in the heat flux trace from $\epsilon = 6$ to $\epsilon = 8$ is mainly caused by an increase in the temperature difference around 367 °CA (from 473 to 688 °C). The difference between the gas and the wall temperature does not increase that strongly any more when the compression ratio is further increased (from 8 to 10). Thus, the increase in the heat flux trace for a higher compression ratio in that region is mainly caused by the faster combustion process and the intensified gas motion. This is reflected in an increase in the peak of the convection coefficient (from 1420 to 1805 W/m^2K).

3.2.3. Variation of the ignition timing

The ignition timing is varied around the MBT-timing to check its influence on the heat transfer, it is advanced and retarded with 12 °CA from MBT. The measured and calculated traces are plotted in Fig. 11 (at P2, $\epsilon = 8$ and $\lambda = 1.5$). There is a significant increase in the peak of the measured heat flux trace with an advanced ignition timing (from 129 to 158 W/cm^2). However, it cannot be concluded which effect causes this increase, because the change in the peak of the temperature difference (from 1455 to 1520 °C) and convection coefficient (from 1335 to 1446 W/m^2K) are not significant if one considers the estimated errors of 6 and 11 %. Consequently, the shift in time of the heat flux is the most important influence of the changing ignition timing.

3.2.4. Variation of the mixture richness

The air-to-fuel equivalence ratio (λ) is varied from 1 to 2. The measured and calculated traces are plotted in Fig. 12 (at P2 and $\epsilon = 8$). The ignition is kept constant again, so there is only a variation in λ. The heat flux increases with a decreasing λ (increasing mixture richness).

Both the convection coefficient and the temperature difference between the gas and the wall increase. There is a larger time difference between the maximum of the convection coefficient and the temperature difference for a lower λ. This causes a more stretched heat flux trace. Consequently, the maximum of the heat flux trace does not occur at the moment of maximum ΔT anymore for $\lambda = 2$. The heat flux does stay at a high level until the temperature difference reaches its maximum. A clear time shift in all three plotted traces can be noted if the mixture gets leaner. This visualizes the effect of the mixture richness on the combustion rate. As the mixture gets leaner, the combustion rate slows down, being enforced by the constant ignition timing.

3.3. A comparison between methane and hydrogen

A comparison is made between the heat transfer of hydrogen and methane measurements with the same indicated engine power output. The measured heat flux, the calculated convection coefficient and the calculated temperature difference between the gas and the wall temperature for two comparable measurements of hydrogen and methane are plotted in Fig. 13. Extra information about the measurements is given in Table 3. The measurements are taken at P2, the compression ratio being equal to 9. The hydrogen measurements have an air-to-fuel equivalence ratio of 1 and 2. The measurements of methane are always stoichiometric and the power output is equalized with the hydrogen measurements by throttling. Ignition is at MBT-timing.

The heat flux of the stoichiometric hydrogen measurement (Fig. 13(a)) is clearly higher than the heat flux of the corresponding methane measurement. However, the lean hydrogen measurement (Fig. 13(b)), has a heat flux which is lower than that of methane. In the case of methane, the heat flux does not decrease a lot when the in-cylinder mass is reduced by throttling. The total cycle heat loss of the measurement with the lowest power output is only 12 % smaller than the one with the highest power output, although the power output is decreased with 26 %. This is also reflected in the increase of ϕ_h from 27 to 30 %. The difference between the two hydrogen measurements is much bigger. The total cycle heat loss decreases with 64 % and ϕ_h with 41 %. The indicated efficiency of the hydrogen measurements increases from 23 to 29 % as a result.

The trace of the temperature difference between the gas and the wall is about the same for the two methane measurements. The reduced in-cylinder mass and pressure cancel each other out in the equation of state. This is the reason why the heat flux does not decrease a lot if the power output is reduced by throttling. The lean hydrogen measurement has a lower peak in the temperature difference and therefore a lower heat flux. Another reason for the decreased heat flux is the slower combustion in the case of the lean hydrogen-air mixture, resulting in a lower convection coefficient.

In the literature it is stated that the heat transfer of hydrogen is higher compared to a fossil fuel (e.g. gasoline [20] or methane [32]). The measurements discussed above show that this is not always the case, the heat loss of hydrogen combustion can be lower if a lean mixture is used.

The results above demonstrate the advantage of hydrogen. A high engine efficiency can be attained at low engine loads because of three reasons. First, there is no need to use a throttle because of the wide flammability limits, resulting in low pumping losses. Second, the heat losses are low because the peak gas temperature of the lean combustion is low. Third, the thermodynamic properties of the working fluid (κ) change, resulting in an increased theoretical efficiency [1].

4. Conclusions

The heat flux and wall temperatures have been measured in a hydrogen-fuelled spark ignited combustion engine under motored and fired conditions. The effect of a variation in the compression ratio, ignition timing and mixture richness has been investigated. A convection coefficient has been calculated in an attempt to separate the effect of the temperature difference between the gas and the wall on the heat transfer from other effects. The heat flux of hydrogen has been compared to a fossil-fuel, in this case methane, to investigate the differences in the heat transfer process. Measurements with the same indicated power output have been compared. This paper has demonstrated that the convection coefficient gives more insight in the heat transfer process, despite the assumptions involved in its definition. However, the motored measurements showed that the convection coefficient can have negative values which indicate that its definition should be adjusted. The main conclusions of the paper are as follows:

- The convection coefficient represents the influence of the combustion process and in-cylinder movement on the heat transfer process. The maximum in the

convection coefficient trace corresponded with the end of the initial rising slope of the measured heat flux for all the measurements. The largest part of the initial increase in the heat flux is caused by the combustion process and the gas movement. The heat flux starts to rise at the instant that the flame front passes over the measurement position. The maximum in the heat flux trace occurred together with the maximum in the temperature difference between the in-cylinder gases and the cylinder wall. This was not the case if the instant between the flame passage and the maximum in the temperature difference was spread too much in time. The maximum in the heat flux trace then corresponded with the maximum in the convection coefficient. The heat flux did remain at a high level until the temperature difference reached its maximum.

- The heat flux increased for an increasing compression ratio. This increase is caused by an increase in the temperature difference between the gas and the wall between a compression ratio of 6 and 8. The increase between a compression ratio of 8 and 10 is mainly caused by an increase in the gas movement and a faster combustion process.
- An advanced ignition timing caused an increase in the heat flux. It is not clear if this is caused by an increase in the temperature difference or the convection coefficient, because these differences were not significant. Consequently, the main influence of the changing ignition timing is that it shifts the traces in time.
- The heat flux and convection coefficient increased with an increasing mixture richness. The comparable measurements between hydrogen and methane have demonstrated that the mixture richness has a large influence on the heat transfer process in a combustion engine. The heat flux decreased significantly if the mixture richness of the hydrogen-air mixture was reduced to operate the engine at a low load. Consequently, the total cycle heat loss decreased, resulting in a higher engine efficiency. Reducing the cylinder mass to lower the engine power output did not have the same effect on the heat flux.

Acknowledgements

The authors of this paper like to acknowledge the suggestions and technical assistance of Koen Chielens and Patrick De Pue. The research is carried out in the framework of a Ph.D. which is funded by a grant (SB-81139) of the Institute for the Promotion of Innovation through Science and Technology in Flanders (IWT-Vlaanderen). The experimental equipment is funded by a Research Grant (1.5.147.10N) of the Research Foundation - Flanders (FWO). These financial supports are gratefully acknowledged. J. Vancoillie acknowledges the Research Foundation - Flanders (FWO) for the Ph.D. grant 09/ASP/030.

References

[1] S. Verhelst, T. Wallner, Hydrogen-fueled internal combustion engines, Progress in Energy and Combustion Science 35 (6) (2009) 490–527. doi:10.1016/j.pecs.2009.08.001.

[2] R. Sierens, S. Verhelst, Influence of the injection parameters on the efficiency and power output of a hydrogen fueled engine, Journal of Engineering for Gas Turbines and Power-Transactions of the ASME 125 (2) (2003) 444–449. doi:10.1115/1.1496777.

[3] S. Verhelst, P. Maesschalck, N. Rombaut, R. Sierens, Increasing the power output of hydrogen internal combustion engines by means of supercharging and exhaust gas recirculation, International Journal of Hydrogen Energy 34 (10) (2009) 4406–4412. doi:10.1016/j.ijhydene.2009.03.037.

[4] S. Verhelst, P. Maesschalck, N. Rombaut, R. Sierens, Efficiency comparison between hydrogen and gasoline, on a bi-fuel hydrogen/gasoline engine, International Journal of Hydrogen Energy 34 (5) (2009) 2504–2510. doi:10.1016/j.ijhydene.2009.01.009.

[5] S. Verhelst, A study of the combustion in hydrogen-fuelled internal combustion engines, Ph. D. thesis, Ghent University - UGent (2005).
URL `http://hdl.handle.net/1854/3378`

[6] S. Verhelst, R. Sierens, A quasi-dimensional model for the power cycle of a hydrogen-fuelled ICE, International Journal of Hydrogen Energy 32 (15) (2007) 3545–3554. doi:10.1016/j.ijhydene.2007.02.011.

[7] P. Puzinauskas, G. Hutcherson, B. Willson, Ignition and boost effects on large-bore engine in-cylinder heat transfer, Applied Thermal Engineering 23 (1) (2003) 1–16.

[8] C. Rakopoulos, D. Rakopoulos, G. Mavropoulos, E. Giakoumis, Experimental and theoretical study of the short term response temperature transients in the cylinder walls of a diesel engine at various operating conditions, Applied Thermal Engineering 24 (5-6) (2004) 679–702.

[9] J. Galindo, J. Lujan, J. Serrano, V. Dolz, S. Guilain, Description of a heat transfer model suitable to calculate transient processes of turbocharged diesel engines with one-dimensional gas-dynamic codes, Applied Thermal Engineering 26 (1) (2006) 66–76.

[10] A. Sanli, A. Ozsezen, I. Kilicaslan, M. Canakci, The influence of engine speed and load on the heat transfer between gases and in-cylinder walls at fired and motored conditions of an idi diesel engine, Applied Thermal Engineering 28 (11-12) (2008) 1395–1404. doi:10.1016/j.applthermaleng.2007.10.005.

[11] M. Lounici, K. Loubar, M. Balistrou, M. Tazerout, Investigation on heat transfer evaluation for a more efficient two-zone combustion model in the case of natural gas SI engines, Applied Thermal Engineering In Press, Accepted Manuscript. doi:10.1016/j.applthermaleng.2010.09.012.

[12] C. Rakopoulos, G. Kosmadakis, E. Pariotis, Critical evaluation of current heat transfer models used in CFD in-cylinder engine simulations and establishment of

a comprehensive wall-function formulation, Applied Energy 87 (5) (2010) 1612–1630.

[13] A. Mohammadi, M. Yaghoubi, Estimation of instantaneous local heat transfer coefficient in spark-ignition engines, International Journal of Thermal Sciences 49 (7) (2010) 1309–1317.

[14] Z. Han, R. Reitz, A temperature wall function formulation for variable-density turbulent flows with application to engine convective heat transfer modeling, International Journal of Heat and Mass Transfer 40 (3) (1997) 613–625.

[15] H. Jung, Development of an in-cylinder heat transfer model with compressibility effects on turbulent prandtl number, eddy viscosity ratio and kinematic viscosity variation, SAE paper 2009-01-0702 (2009).

[16] J. Chang, O. Guralp, Z. Filipi, D. Assanis, New heat transfer correlation for an HCCI engine derived from measurements of instantaneous surface heat flux, SAE paper 2004-01-2996 (2004).

[17] M. Garcia, F. Aguilar, T. Lencero, J. Villanueva, A new heat release rate (HRR) law for homogeneous charge compression ignition (HCCI) combustion mode, Applied Thermal Engineering 29 (17-18) (2009) 3654–3662.

[18] H. Soyhan, H. Yasar, H. Walmsley, B. Head, G. Kalghatgi, C. Sorusbay, Evaluation of heat transfer correlations for HCCI engine modeling, Applied Thermal Engineering 29 (2-3) (2009) 541–549.

[19] T. Shudo, H. Suzuki, Applicability of heat transfer equations to hydrogen combustion, JSAE Review 23 (3) (2002) 303–308.

[20] S. Wei, A study on transient heat transfer coefficient of in-cylinder gas in the hydrogen fueled engine, in: KHES and HESS, the 6th Korea-Japan Joint Symposium on Hydrogen Energy, 2001, p. 10.

[21] J. Demuynck, M. De Paepe, H. Huisseune, R. Sierens, J. Vancoillie, S. Verhelst, On the applicability of empirical heat transfer models for hydrogen combustion engines, International Journal of Hydrogen Energy Accepted manuscript, In Press. doi:10.1016/j.ijhydene.2010.10.059.

[22] M. Marr, J. Wallace, S. Chandra, L. Pershin, J. Mostaghimi, A fast response thermocouple for internal combustion engine surface temperature measurements, Experimental Thermal and Fluid Science 34 (2) (2010) 183–189.

[23] J. Demuynck, S. Pauwels, S. Verhelst, M. De Paepe, R. Sierens, Experimental research on the heat transfer inside a hydrogen combustion engine: Evaluation and construction of measurement methods, in: Proceedings of the FISITA 2008 World Automotive Congress. (F2008-SC-037), Munich, Germany, 2008.

[24] J. Demuynck, N. Raes, M. Zuliani, M. De Paepe, R. Sierens, S. Verhelst, Local heat flux measurements in a hydrogen and methane spark ignition engine with a thermopile sensor, International Journal of Hydrogen Energy 34 (24) (2009) 9857–9868. doi:10.1016/j.ijhydene.2009.10.035.

[25] B. Tillock, J. Martin, Measurement and modeling of thermal flows in an air-cooled engine, SAE paper 961731 (1996).

[26] W. Bauer, J. Wenisch, J. Heywood, Averaged and time-resolved heat transfer of steady and pulsating entry flow in intake manifold of a spark-ignition engine, International Journal of Heat and Fluid Flow 19 (1) (1998) 1–9.

[27] A. Wimmer, R. Pivec, T. Sams, Heat transfer to the combustion chamber and port walls of IC engines - measurement and prediction, SAE paper 2000-01-0568 (2000).

[28] W. Annand, Heat transfer in the cylinders of reciprocating internal combustion engines, Proc Instn Mech Engrs 177 (36) (1963) 973–996.

[29] J. Taylor, An introduction to error analysis: the study of uncertainties in physical measurements, University Science Books, 1982.

[30] Vatell, Heat flux microsensor manual (2010).
URL `http://www.vatell.com/hfm.htm`

[31] J. Heywood, Internal Combustion Engine Fundamentals, McGraw-Hill, 1988.

[32] T. Shudo, Y. Nakajima, T. Futakuchi, Thermal efficiency analysis in a hydrogen premixed combustion engine, JSAE Review 21 (2) (2000) 177–182.

Table 1: Geometrical properties and valve timing of the CFR engine

Bore	82.55 mm
Stroke	114.2 mm
Connecting rod length	254 mm
Swept volume	611.7 cm^3
IVO	17 °CA ATDC
IVC	26 °CA ABDC
EVO	32 °CA BBDC
EVC	6 °CA ATDC

Table 2: The accuracy of the measurement equipment

Variable	Device	Accuracy
Heat flux gain	Vatell AMP-6	±3.6%
Wall temperature gain	Vatell AMP-6	±1.5%
In-cylinder pressure	Kistler 701A	±1%
Intake manifold pressure	Kistler 4075A20	±2.5%
Air flow rate	Bronkhorst F-106BZ	$\pm 1\% FS$
Hydrogen flow rate	Bronkhorst F-201AC	$\pm 1\% FS$
Engine speed	ASTM tachometer	±6 rpm
Atmospheric temperature		±0.5 °C
Atmospheric pressure		±50 Pa

Table 3: Comparison between comparable measurements of hydrogen and methane plotted in Fig. 13

fuel	λ	throttle	Q_{fuel} (J)	W_i (J)	η_i (%)	Q_h (J)	ϕ_h (%)
hydrogen	1	WOT	1629	374	23	609	37
methane	1	pos 74°	1412	372	26	379	27
hydrogen	2	WOT	988	284	29	220	22
methane	1	pos 78°	1091	276	25	332	30

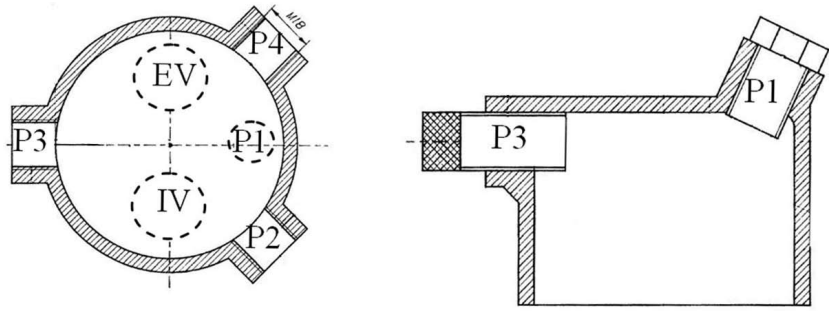

Figure 1: Cross-section of the CFR engine, P1: spark plug, P1-P4: sensor positions, IV: intake valve, EV: exhaust valve

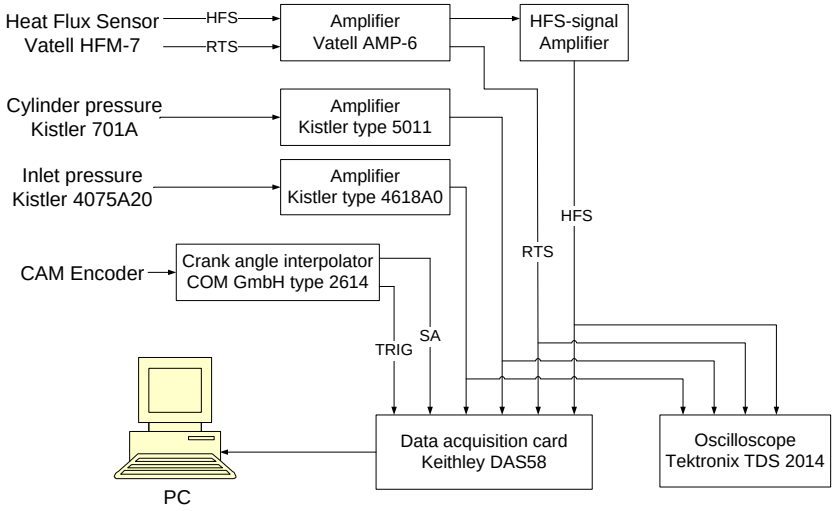

Figure 2: Measuring equipment, HFS: heat flux signal, RTS: substrate temperature signal, TRIG: trigger signal every two cycles, SA: sample signal every 0.5 °CA

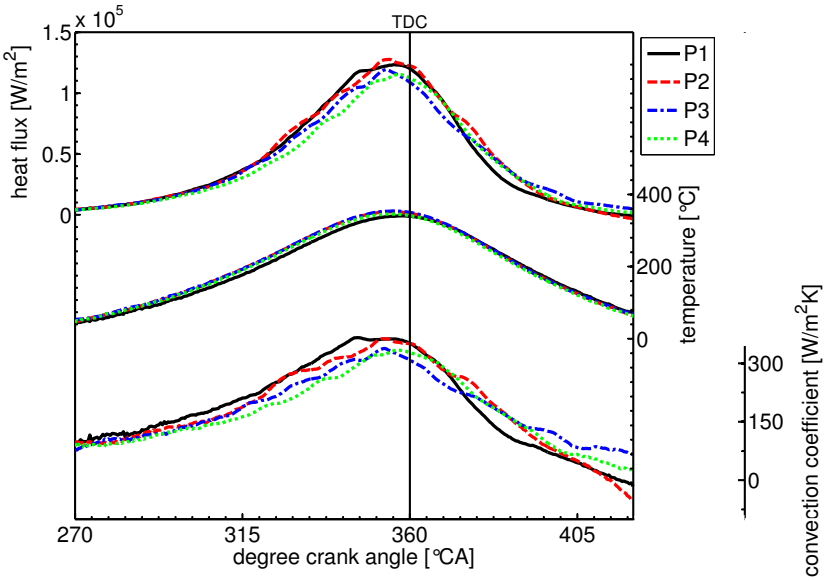

Figure 3: There are only small differences in the heat flux between the different measurement positions under motored operation (CR=10, WOT)

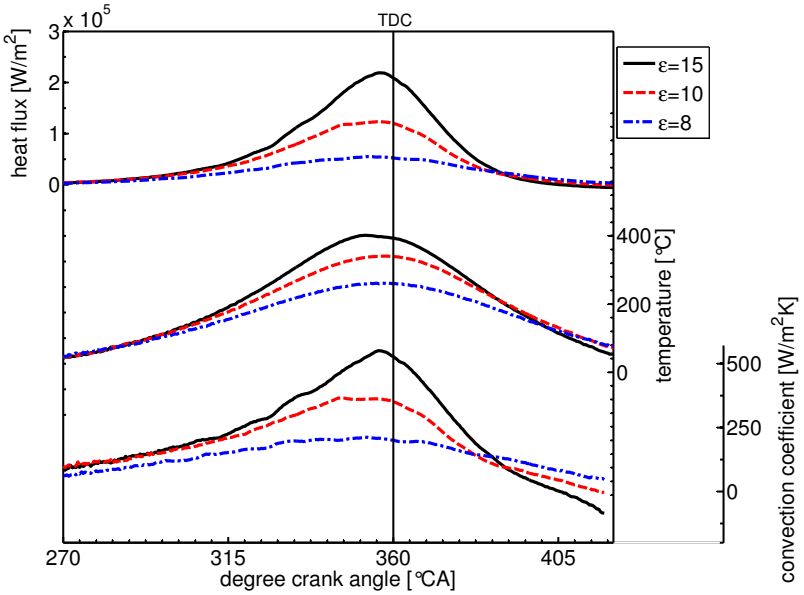

Figure 4: There is an increase in the traces of q, ΔT and h around TDC if the compression ratio rises (P1, WOT). The trend is the other way around near the end of the expansion stroke.

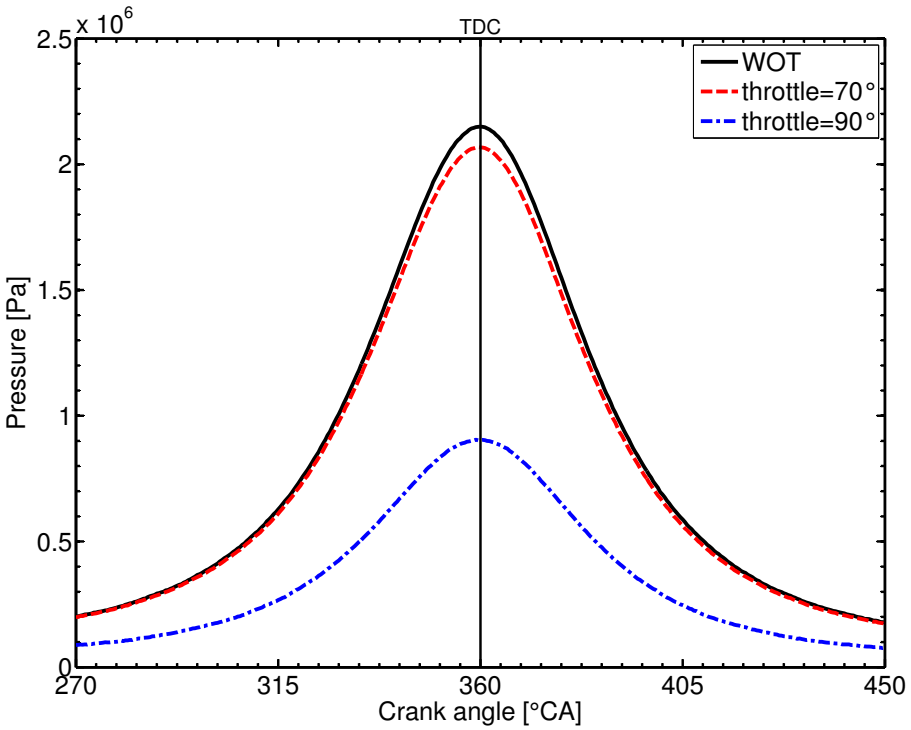

Figure 5: A throttle in the intake manifold is used to reduce the in-cylinder mass (P1, $\epsilon = 10$).

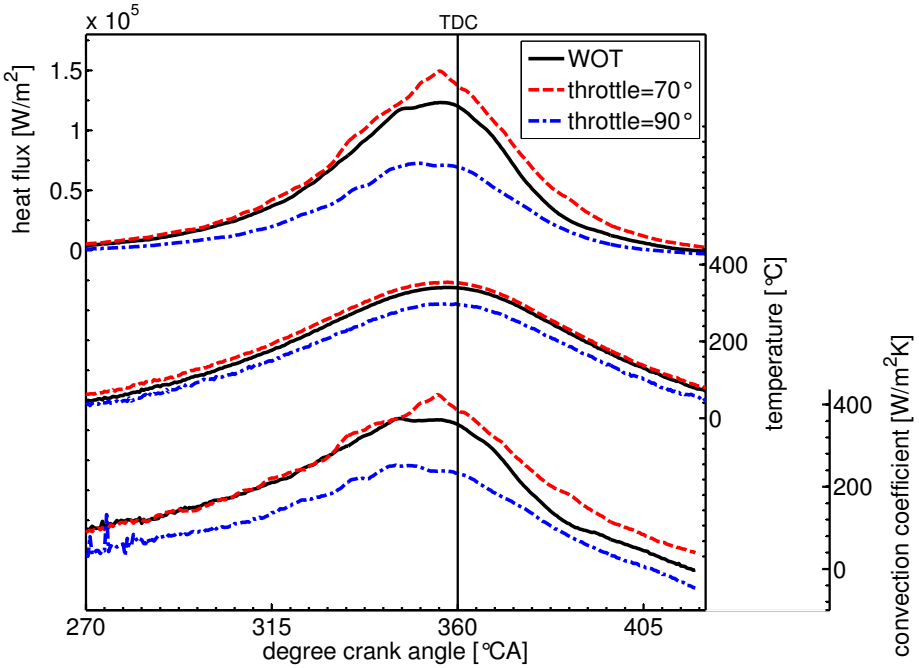

Figure 6: The throttle induces turbulence, which causes the heat flux to increase until a position of 70° (P1, $\epsilon = 10$). Further throttling reduces the heat flux.

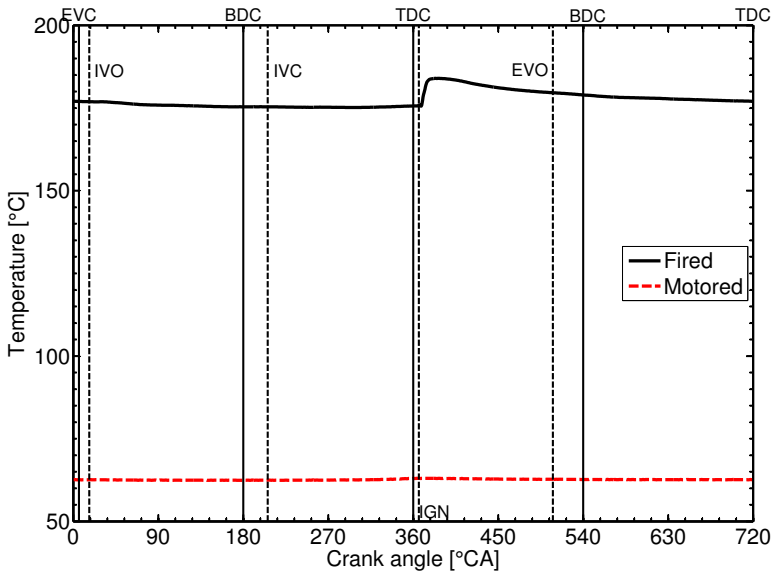

Figure 7: The wall temperature of the cylinder typically increases by 5 to 10 °C during the combustion period (P2, $\epsilon = 8$, $\lambda = 1$, IGN=MBT), whereas under motored operation it almost remains constant.

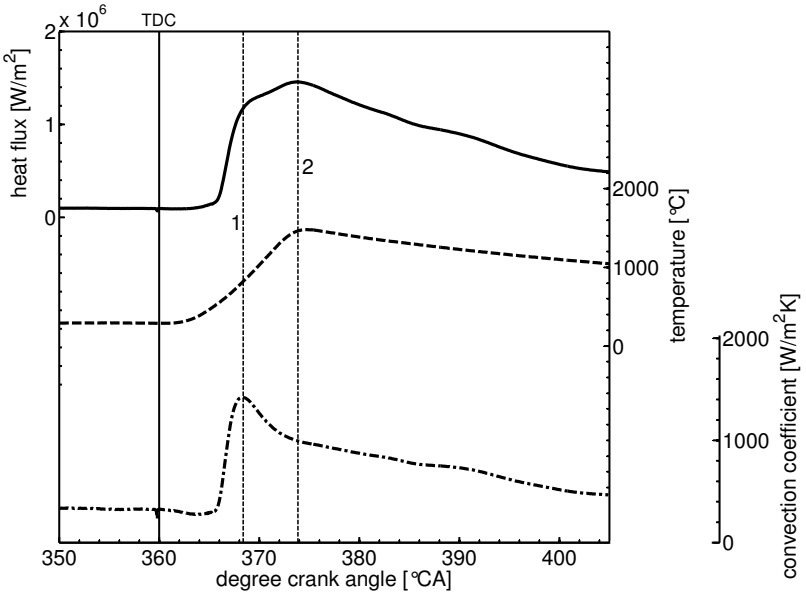

Figure 8: The heat flux peaks when the temperature difference reaches its maximum, see line 2 (P2, $\epsilon = 8$, $\lambda = 1.5$ and IGN=TDC). The end of the initial steep rise in the heat flux coincides with the maximum of the convection coefficient (line 1).

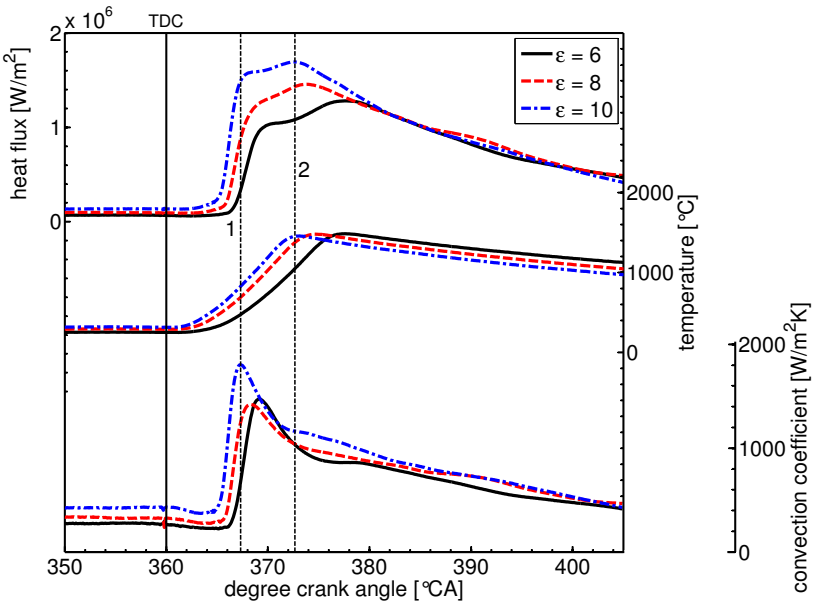

Figure 9: A higher compression ratio results in an increasing heat flux (P2, $\lambda = 1.5$ and IGN=TDC). There is a different trend in the trace of the convection coefficient between an ϵ of 6 and 8 compared to between 8 and 10.

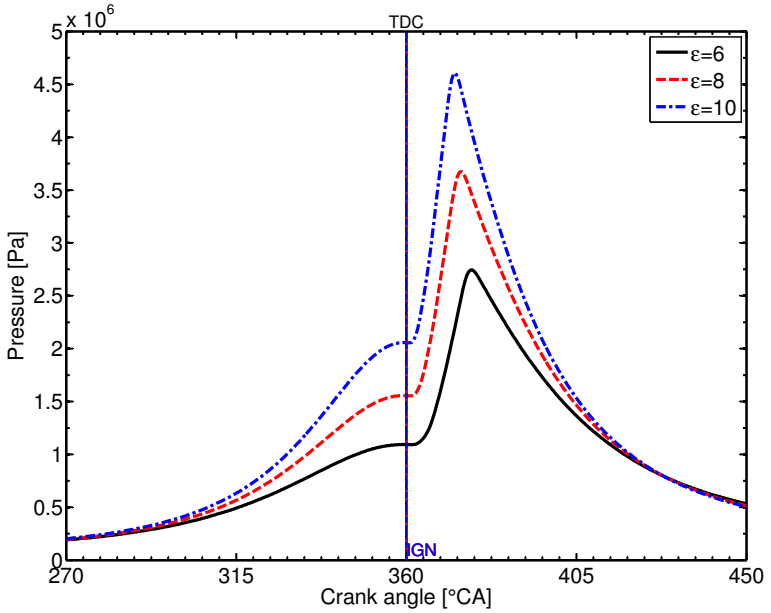

Figure 10: A higher compression ratio results in an increasing cylinder pressure (P2, $\lambda = 1.5$ and IGN=TDC).

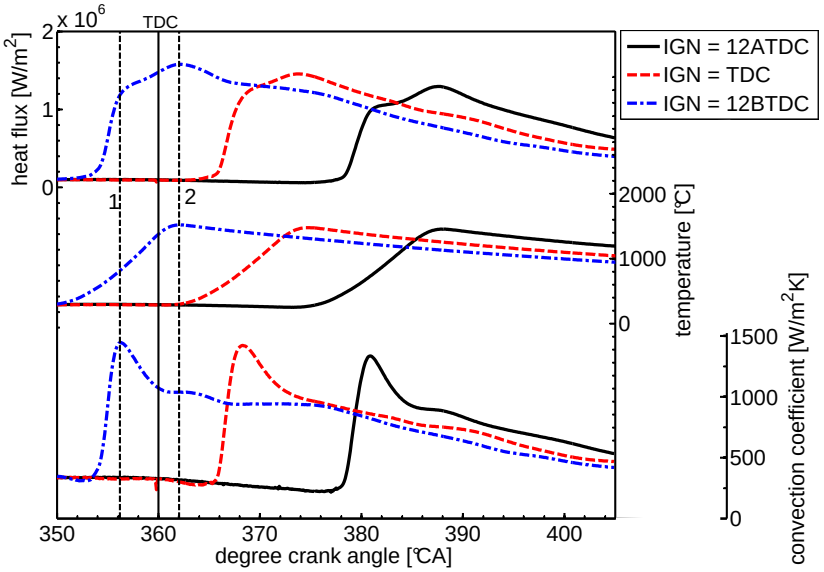

Figure 11: The most important change in the heat flux caused by a varying ignition timing is the shifting in time (P2, $\epsilon = 8$, $\lambda = 1.5$). The differences in the traces of ΔT and h are not significant if one considers the measurement uncertainties.

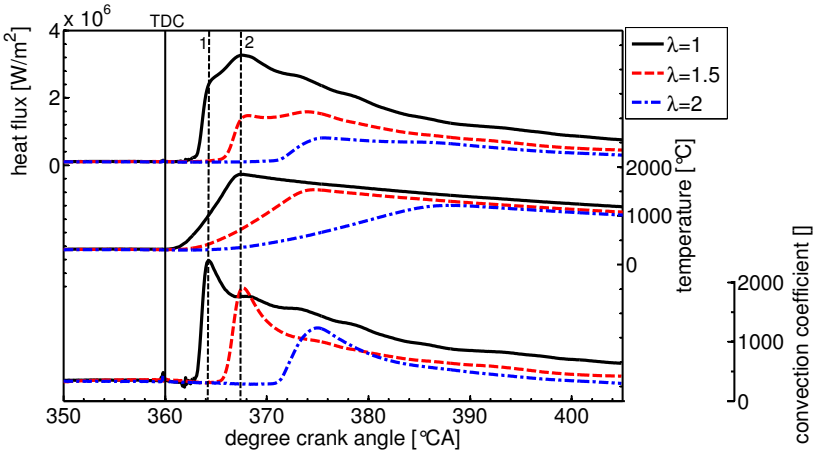

Figure 12: The heat flux increases with an increasing mixture richness. Both the convection coefficient and the temperature difference between the gas and the wall increase, ($P2$,$\epsilon = 8$,$IGN = TDC$).

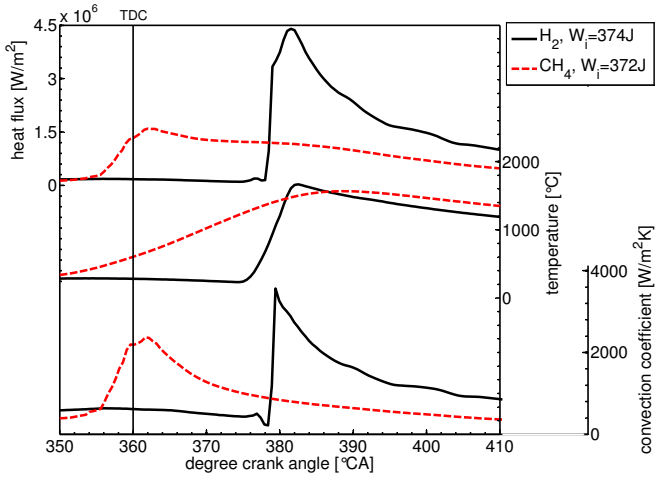

(a) The heat flux of hydrogen at a high power output is much higher compared to methane, resulting in a lower engine efficiency

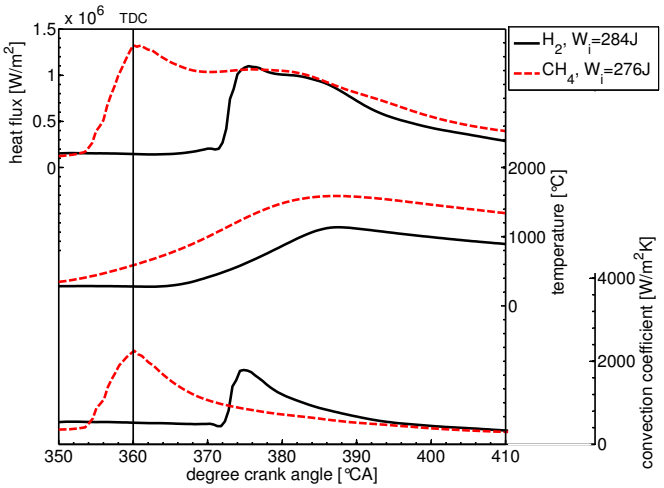

(b) The mixture richness has a large influence on the heat flux. The heat flux of hydrogen becomes lower than that of methane at a low power output which results in a higher engine efficiency.

Figure 13: The heat flux of hydrogen and methane measurements with the same indicated power output are compared (P2, $\epsilon = 9$, IGN=MBT).